A combined finite element-Langevin dynamics (FEM-LD) approach for analyzing the mechanical response of bio-polymer networks

Yuan Lin[1,*], X. Wei[1], J. Qian[2], K.Y. Sze[1] and V.B. Shenoy[3,*]

[1] Department of Mechanical Engineering, The University of Hong Kong, Hong Kong SAR, China

[2] Department of Engineering Mechanics, Zhejiang University, Hangzhou, Zhejiang, China

[3] Department of Materials Science and Engineering, University of Pennsylvania, Philadelphia, PA 19104, USA

[*]Corresponding authors: ylin@hku.hk, vshenoy@seas.upenn.edu

June 8, 2013

Abstract

A Langevin dynamics based formulation is proposed to describe the shape fluctuations of biopolymer filaments. We derive a set of stochastic partial differential equations (SPDEs) to describe the temporal evolution of the shape of semiflexible filaments and show that the solutions of these equations reduce to predictions from classical modal analysis. A finite element formulation to solve these SPDEs is also developed where, besides entropy, the finite deformation of the filaments has been taken into account. The validity of the proposed finite element-Langevin dynamics (FEM-LD) approach is

verified by comparing the simulation results with a variety of theoretical predictions. The method is then applied to study the mechanical behavior of randomly cross-linked F-actin networks. We find that as deformation progresses, the response of such network undergoes transitions from being entropy dominated to being governed by filament bending and then, eventually, to being dictated by filament stretching. The levels of macroscopic stress at which these transitions take place were found to be around 1 and 10 percent, respectively, of the initial bulk modulus of the network, in agreement with recent experimental observations.

Introduction

It is well known that bio-filaments like F-actin and microtubules are responsible for key functions of cells such as maintaining their shape (Preston et al., 1990), driving movement (Theriot and Mitchison, 1991), and mechanosensing (Mattila and Lappalainen, 2008). As such, extensive efforts have been directed over the last decade to uncover how networks composed of these bio-polymer filaments resist deformation and how this load bearing capability correlates with factors like network architecture (Gardel et al., 2004; Tharmann et al., 2007; Chaudhuri et al., 2007; Liu et al., 2008), the properties of cross-linking proteins (Wagner et al., 2006; Lieleg et al., 2008; Lieleg et al., 2009), and the appearance of myosin molecular motors (Koenderink et al., 2009). For example, it has been shown that like most other polymeric materials, the shear modulus of a random in vitro actin network increases significantly with applied stress (Gardel et al., 2004; Tharmann et al., 2007). In contrast, it was reported that a branched network, consisting of short actin filaments, will actually undergo stress softening after an initial hardening stage (Chaudhuri et al., 2007). It is commonly believed that the phenomenon of stress-stiffening originates from the fact that, close to its

contour length, increasing force has to be applied to a semi-flexible chain, against thermal undulations. Theoretically, based on proper descriptions of the behavior of a single filament, various constitutive models have been proposed by invoking assumptions about the nature of the deformation and/or the architecture of the network. For example, simple theories on how rubber-like materials (Mark and Erman, 1988) or biological gels (Storm et al., 2005) respond to deformation have been developed under the assumption that the structure distorts in an affine manner (i.e. all filaments strain uniformly). Similarly, constitutive laws describing the multiaxial stress-strain behavior of these materials have also been proposed (Arruda and Boyce, 1993; Palmer and Boyce, 2008) by adopting the so-called Arruda-Boyce model where the unit cell of the network is assumed to have eight cross-linked chains.

Trying to avoid making a priori assumptions, such as that the deformation is uniform or the network has a specific unit cell structure, direct simulations on computer generated networks have received increasing attention. For example, numerical simulations on two dimensional networks consisting of straight filaments have revealed that the deformation is not affine at small strains (Head et al., 2003a; 2003b; Wilhelm and Frey, 2003). Subsequently, finite element (FEM) simulations (Onck et al., 2005; Huisman et al., 2007) suggested that the stress-stiffening of a filament network is actually caused by the fact that at small levels of applied strains, deformation can easily be accommodated by filament bending, however, as strain increases, more filaments will begin to stretch, which ultimately leads to an increased resistance against deformation. Recently, by treating myosin motors as force dipoles, the influence of such molecular motors on the response of actin networks has also been examined (Chen and Shenoy, 2010) via FEM simulations. One thing we must point out is that thermal undulations of individual filaments have not really been taken into account in the aforementioned computational investigations. The only attempt to our knowledge to include this

effect was made by Onck et al. (2005), where a curved shape was assigned to each filament at the beginning of simulation (prior to mechanical loading) to represent the influence of thermal fluctuations. This approach however is not realistic as the filament shape evolves continuously under the influence of thermal excitations.

The entropy-driven deformation and fluctuations of polymers are usually studied via Brownian dynamics (BD) simulations where the molecule is treated as a series of beads interconnected by springs or rods with a set of stochastic forces acting on each bead to represent thermal fluctuations (Doi and Edwards, 1994). However, among many other issues, a large number of degrees of freedom is needed in such an approach to accurately capture the bending and shear effects of realistic structures. Recently, the finite element method has been used in conjunction with the BD approach to overcome this deficiency where the polymer is essentially modeled as an elastic beam (Cyron and Wall, 2009; 2010). It has been demonstrated that simulation results from this approach can match well with experimental observations and theoretical predictions like the diffusion coefficient and end-to-end distance of the molecule. Despite these promising advances, several important issues remain unsettled here. First, on a fundamental level, the validity of the Brownian (or Langevin) dynamics approach has not been rigorously benchmarked against other theoretical methods. For example, modal analysis has been extensively used throughout the literature to examine the thermal undulations of soft objects like bio-polymers (MacKintosh et al., 1995; Marko and Siggia, 1995) and lipid membranes (Milner and Safran, 1987; Lin et al., 2007). However, the equivalence or a possible relationship between this analytical approach and the Brownian dynamics description has not been established. We also feel that special attention should be paid to the difference between the transverse and longitudinal motions of a semi-flexible molecule. For example, the viscous coefficients associated with the transverse and axial

movements of a polymer segment were taken to be of the same order of magnitude in (Cyron and Wall, 2009; 2010), a treatment that, to us, might not be that appropriate for analyzing the mechanical response of filaments. In addition, as pointed out earlier, it seems that thermal excitations have not really been included in previous FEM simulations on the behavior of realistic filament networks.

Aiming to address these issues, a Langevin dynamics based formulation is developed here to describe the shape fluctuations of bio-polymers. We show that, solutions of the resulting stochastic partial differential equation (SPDE) asymptotically reduce to the predictions from classical modal analysis for simple problems and hence unambiguously prove the validity of this approach. This formulation is then implemented in a finite element framework where, in addition to entropy, the finite deflection of filament has also been included. The validity of the proposed finite element-Langevin dynamics (FEM-LD) approach is verified by comparing the simulation results with various theoretical predictions. Finally, as a numerical example, our method is used to investigate the mechanical response of a random network consisting of numerous actin filaments. Our results clearly demonstrate how the response of the network changes from being entropy dominated to being governed by filament bending and then, eventually, to being dictated by filament stretching as deformation increases. In addition, the levels of macroscopic stress at which the aforementioned transitions take place were found to be around 1 and 10 percent, respectively, of the initial bulk modulus of the network, in consistent with recent experimental observations.

Formulation

Consider a filament immersed in a thermal bath as shown in Fig. 1. Due to the bombardment of molecules from the surrounding medium, the filament is expected to undergo continuous fluctuations in its shape. According to Langevin (Coffey et al., 2004), the effects of collisions with surrounding fluid molecules on the motion of any particle can be represented by (i) a viscous force ξV, with V and ξ being the particle velocity and the medium viscosity respectively, thwarting the movement of the object, and (ii) a random force f driving the Brownian motion of that particle. Furthermore, the random force must follow a Gaussian distribution with zero mean and, in the one dimensional case, satisfy the relation, $< f(t) \;\; f(\tau) >= 2\xi k_B T \delta(t-\tau)$, where t and τ represent time, δ corresponds to the Dirac delta function, and $k_B T$ is the thermal energy. The same line of reasoning can be applied to analyzing thermal undulations of extended objects like filaments and membranes. The only difference is that, for a filament (treated as a beam here), f must be interpreted as a distributed load causing the beam to deflect and ξ should represent the viscous coefficient per unit length of the filament. In addition, the relationship between f and ξ becomes

$$< f(\vec{x},t) \quad f(\vec{y},\tau) >= 2\xi k_B T \delta(\vec{x}-\vec{y})\delta(t-\tau). \tag{1}$$

Hence, neglecting effects of inertia, the thermal fluctuations of an initially straight filament can be described by

$$\xi \frac{\partial w}{\partial t} + EI \frac{\partial^4 w}{\partial x^4} = f(x,t) \tag{2}$$

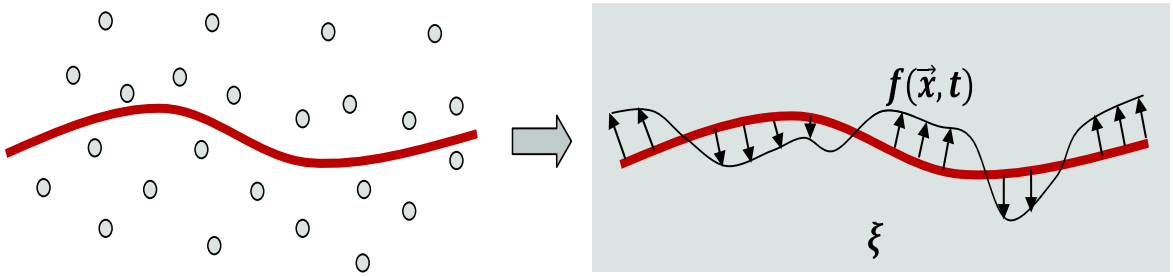

Figure 1: A filament immersed in a thermal reservoir undergoes shape fluctuations. The effects of bombardment of water molecules on the motion of the filament can be represented by a macroscopic medium viscosity ξ and a distributed random load f.

where EI is the bending rigidity of the filament and w is the deflection of the beam, refer to Fig. 2. We want to point out that (2) is a stochastic partial differential equation (SPDE) since the force f is random. If both ends of the beam (with length L) are simply supported, as shown in Fig. 2, then the solution of (2), satisfying the initial condition $w(x,0)=0$, can be found as

$$w(x,t)=\frac{2}{L\xi}\sum_n \sin\frac{n\pi x}{L}\int_0^L \sin\frac{n\pi s}{L}\int_0^t f(s,\tau)e^{-n^4\pi^4 EI(t-\tau)/\xi L^4}d\tau ds, \tag{3}$$

from which the correlation function of w can be obtained as

$$< w(x,t)\quad w(y,\eta) >= \frac{2k_BTL^3}{\pi^4 EI}\sum_n \frac{\sin(n\pi x/L)\sin(n\pi y/L)}{n^4}\left[e^{-n^4\pi^4 EI(\eta-t)/\xi L^4}-e^{-n^4\pi^4 EI(\eta+t)/\xi L^4}\right] \tag{4}$$

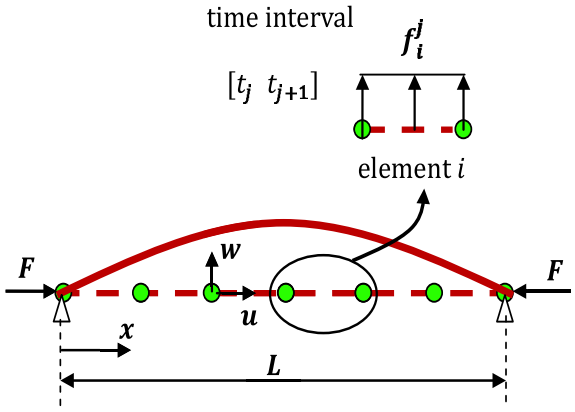

Figure 2: Schematic plot of a simply supported filament. The solid line corresponds to the deformed beam induced by thermal excitations. The un-deformed filament is represented by the dashed line. The deflection and axial displacements of the filament are denoted as w and u, respectively. Following standard FEM procedure, the un-deformed beam is divided into numerous equal-sized segments. To represent the effect of thermal fluctuations, a constant load f_i^j acting on element i during the time interval from t_j to t_{j+1} must be introduced according to Eq. (8).

where, without loss of generality, it is assumed $\eta \geq t$. In the limiting case where $y = x$, $\eta = t$, and $t \to \infty$, (4) reduces to

$$\lim_{t\to+\infty} < w(x,t) \quad w(x,t) >= \sum_n \frac{2k_BTL^3}{\pi^4 n^4 EI} \sin^2(n\pi x/L). \tag{5}$$

Notice that, following traditional modal analysis approach, the deflection profile can be expressed as $w(x,t) = \sum_n a_n(t) \sin\frac{n\pi x}{L}$ with a_n being a set of random variables. The correlation function shown in (5) implies that

$$< a_n^2 >= \frac{2k_BTL^3}{\pi^4 n^4 EI}, \tag{6}$$

a relationship that can also be arrived if the theorem of equi-partition is invoked (notice that $< a_n >= 0$). However, we want to point out that, unlike traditional modal analysis which produces relationships that are valid only when thermodynamic equilibrium is reached, i.e. over long time periods, the Langevin approach can provide us temporal as well as spatial correlation functions (like (4)) which fully describe the dynamics of the system. More importantly, we believe that the Langevin dynamics formulation provides a viable solution to the outstanding question of how to account for thermally-induced deformations of soft objects in finite element (FEM) simulations.

Implementation in FEM simulations

Let us start with a beam with both ends hinged as shown in Fig. 2. Following standard procedures in FEM, we divide the filament, in the un-deformed configuration, into equally spaced elements. To study thermal fluctuations, we have to first determine a consistent way of applying loads to each element. The simplest choice is to assume that the load acting on element i over the time interval $[t_j \;\; t_{j+1}]$ is uniform and is denoted as f_i^j. To be self-consistent, f_i^j should satisfy

$$f_i^j = \frac{1}{(x_{i+1} - x_i)(t_{j+1} - t_j)} \int_{x_i}^{x_{i+1}} \int_{t_j}^{t_{j+1}} f(x,t) dt dx \tag{7}$$

where x_i and x_{i+1} are the coordinates of the two ends of the element. Obviously, we have $< f_i^j >= 0$. In addition, the so-called auto correlation function of this force can be found as

$$< f_i^j \;\; f_i^j >= \frac{2\xi k_B T}{\Delta x \Delta t}, \tag{8}$$

with $\Delta x = x_{i+1} - x_i$ being the element size and $\Delta t = t_{j+1} - t_j$ being the size of the time step. Hence, the effective force acting on each element follows a Gaussian distribution with a mean of 0 and a variance of $\frac{2\xi k_B T}{\Delta x \Delta t}$. For a given deflection profile at time step j, i.e. w^j, the velocity field at that moment $\dot{w}^j$, predicted by (2), can be determined from

$$\sum_i \int_{x_i}^{x_{i+1}} \left[EI \frac{d^2 w^j}{dx^2} \delta \left(\frac{d^2 w^j}{dx^2} \right) + (\xi \dot{w}^j - f_i^j) \delta w^j \right] dx = 0 \tag{9}$$

where the symbol δ here represents a small variation. Assuming $w^j(x) = \phi_1(x) w_i^j + \phi_2(x) \theta_i^j + \phi_3(x) w_{i+1}^j + \phi_4(x) \theta_{i+1}^j$ in element i with $\theta = -dw/dx$ and ϕ being the standard cubic interpolation functions (Reddy, 1993), (9) reduces to

$$\sum_i \delta \chi_m^j \left[M_{mn} \dot{\chi}_n^j + K_{mn} \chi_n^j - F_m \right] = 0 \tag{10}$$

where $\chi^j = [w_i^j \;\; \theta_i^j \;\; w_{i+1}^j \;\; \theta_{i+1}^j]^T$ and repeated index in the subscript means summation over that index. The force vector $\mathbf{F}$ and two matrices $\mathbf{M}$ and $\mathbf{K}$ introduced here are defined as $F_m = \int_{x_i}^{x_{i+1}} f_i^j \phi_m(x) dx$, $M_{mn} = \int_{x_i}^{x_{i+1}} \xi \phi_m(x) \phi_n(x) dx$, and $K_{mn} = \int_{x_i}^{x_{i+1}} EI \frac{d^2 \phi_m}{dx^2} \frac{d^2 \phi_n}{dx^2} dx$, refer to [25] for the explicit forms of these so-called element matrices/vectors. Once $\dot{\chi}_m^j$ is calculated from (10), the deflection field at time step $j+1$ can be updated as

$$\chi_m^{j+1} = \chi_m^j + \Delta t \cdot \dot{\chi}_m^j. \tag{11}$$

Dividing the beam into 10 equal-sized segments, calculations are carried out for a filament with $\frac{EI}{k_B T L} = 100$ (corresponding to short F-actin of length ~ 120 nm). The mean square of filament deflection at mid-point, i.e. $< w(L/2)^2 >$, is plotted in Fig. 3 for three independent simulations. In comparison, theoretical prediction of this quantity from (5) is

also shown in Fig. 3. Clearly, despite fluctuations, simulation results are found to converge to this theoretical value.

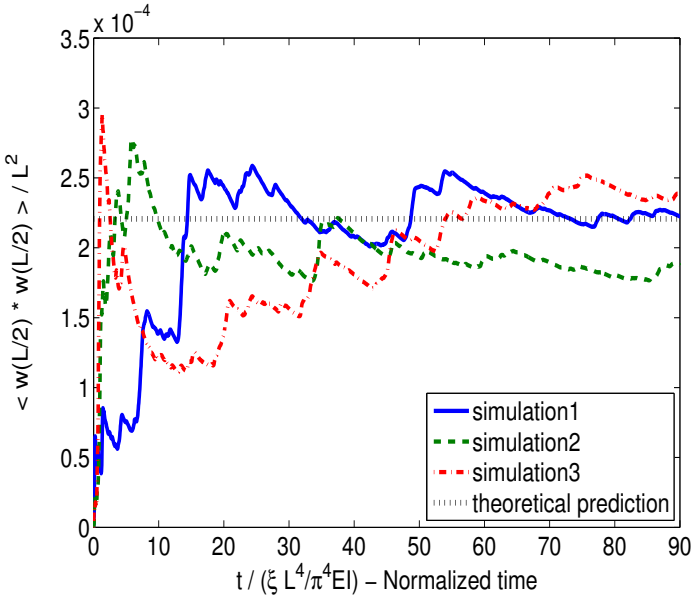

Figure 3: Mean-square of filament deflection at mid-point obtained from three independent FEM-LD simulations. For comparison, prediction from classical modal analysis is also shown by the dotted line. The dimensionless parameter $\frac{EI}{k_B T L}$ is chosen to be 100 in the calculation.

Strategy for finite deflections

All the discussions thus far focused on a single filament with the assumption that the deflections are small (refer to (2)). However, obviously a network may undergo finite or even large deformations in practical situations. Furthermore, buckling can easily take place in individual filaments within the network even if the bulk deformation is small. To capture these phenomena in FEM, we have to include possible displacement of the filament in its axial direction, that is $u(x)$ as illustrated in Fig. 2, in our formulation. Specifically, the

elastic energy stored in, for example, element i in this case takes the form

$$U^i_{elem} = \int_{x_i}^{x_{i+1}} \left[\frac{EA}{2} \left(\frac{du}{dx} + \frac{1}{2} \left(\frac{dw}{dx} \right)^2 \right)^2 + \frac{EI}{2} \left(\frac{d^2w}{dx^2} \right)^2 \right] dx \tag{12}$$

where the first term in the bracket represents the stretching energy with EA being the stretching rigidity of the filament and the second term corresponds to the conventional bending energy. Notice that a nonlinear term $\frac{1}{2}\left(\frac{dw}{dx}\right)^2$ has been included in the axial strain expression here which is often referred to as the von Karman strain (Reddy, 2004).

Before proceeding any further, we have to consider how fast a filament segment moves in the axial direction in comparison with its transverse motion. By definition, the quantity ξV represents the drag force acting on a filament segment of unit length moving transversely with a speed V. Similarly, the frictional force induced by the movement of such segment along the longitudinal direction (with the same speed V) is $\xi_{ax} V$, where ξ_{ax} is the viscous coefficient associated with the axial motion. Notice that we are considering a segment *within* the filament (i.e. not an *isolated* rod) here, so, theoretically, we believe that ξ and ξ_{ax} can be estimated by examining the steady-state viscous flow around an infinite cylinder. The value of ξ has been found to be of the order of $4\pi\mu$ with μ being the coefficient of viscosity of the fluid (Tritton, 1988; Ockendon and Ockendon, 1995). In comparison, direct calculations suggest that ξ_{ax} should be much smaller than ξ, refer to the Appendix A. Physically, this means that u is a fast variable when compared with w, and hence we can assume that u relaxes rapidly to equilibrium, a treatment that, in our opinion, is more appropriate for analyzing the mechanical response of bio-filaments or filament networks (see Appendix A for details). Based on these considerations, a numerical scheme has been developed as follows

- For given displacements at time step j, denoted as w^j and u^j, calculate w^* and u^*

from

$$\sum_i \int_{x_i}^{x_{i+1}} \left[EA \left(\frac{du^*}{dx} + \frac{1}{2} \left(\frac{dw^j}{dx} \right)^2 \right) \delta(du^*/dx) - f_u^{ext} \delta u^* \right] dx = 0, \quad w^* = w^j \quad (13)$$

where f_u^{ext} corresponds to possible external load in the axial direction. Adopting a linear interpolation of u, that is assuming $u(x) = \psi_1(x)u_i + \psi_2(x)u_{i+1}$ in element i with ψ being standard linear interpolation functions as shown in the Appendix B, and a cubic interpolation of w, like before, (13) can be rewritten as

$$\sum_i \delta\chi_m^* \left[K_{mn}\chi_n^* + A_{mn}\chi_n^j + B_{mnr}\chi_n^j\chi_r^j - F_m^u \right] = 0 \quad (14)$$

with $\chi^* = [u_i^* \;\; w_i^* \;\; \theta_i^* \;\; u_{i+1}^* \;\; w_{i+1}^* \;\; \theta_{i+1}^*]^T$ being a 6×1 vector, containing all degrees of freedom associated with the two nodal points of element i, and summation over repeated index in the subscript is assumed. $\mathbf{K}$, $\mathbf{A}$, $\mathbf{B}$ and $\mathbf{F}^u$ introduced here are of dimensions 6×6, 6×6, $6 \times 6 \times 6$ and 6×1, respectively, with components given in the Appendix B. Notice that (13) implies $w^* = w^j$ while u^* in general will be different from u^j to enforce equilibrium in the longitudinal direction, which is consistent with the previous conclusion that u is a fast variable when compared to w. Proper boundary conditions on χ^* will be enforced when solving (14). Essentially, what we have done here is that we "freeze" deflections of filaments while allowing axial displacements to vary freely so as to attain equilibrium in the longitudinal direction. As a result, w^* is *not* an equilibrated value and that is why a non-vanishing contribution $\frac{dw^*}{dt}$ will be generated as discussed in the next step. In addition, u^* calculated here will not

depend on u^j, reflecting the fact that, compared to the transverse motion, the axial movement of filament is taken to be infinite fast and hence equilibrium can be achieved "instantaneously" in that direction.

- Calculate $\dot{w}^*$ and $\dot{u}^*$ from

$$\sum_i \int_{x_i}^{x_{i+1}} \left[EI \frac{d^2 w^*}{dx^2} \delta \left(\frac{d^2 w^*}{dx^2} \right) + EA \left(\frac{du*}{dx} \frac{dw*}{dx} + \frac{1}{2} \left(\frac{dw*}{dx} \right)^3 \right) \delta \left(\frac{dw^*}{dx} \right) + (\xi \dot{w}^* - f_i^j - f_w) \delta w^* \right] dx = 0 \tag{15}$$

and

$$\dot{u}^* = 0. \tag{16}$$

where again f_i^j is the random force acting on element i at time step j, given by (8), and f_w is the summation of externally applied transverse load and internally generated forces acting on junction points within the network, refer to the Appendix B. The matrix (or index) form of (15) and (16) can be expressed as

$$\sum_i \delta \chi_m^* \left[M_{mn} \dot{\chi}_n^* + C_{mn} \chi_n^* + D_{mnr} \chi_n^* \chi_r^* + E_{mnrs} \chi_n^* \chi_r^* \chi_s^* - F_m^w \right] = 0 \tag{17}$$

with expressions of $\mathbf{M}, \mathbf{C}, \mathbf{D}, \mathbf{E}$ and $\mathbf{F}^w$ given in the Appendix B. Boundary conditions on $\dot{\chi}^*$ will be invoked in solving (17).

- Determine the values of all variables at time step $j+1$ by

$$\chi_m^{j+1} = \chi_m^* + \Delta t \cdot \dot{\chi}_m^*. \tag{18}$$

Starting from a given initial state, the whole calculation is carried out by repeating the three steps listed above. Several points regarding this scheme need to be highlighted here: (i) despite the appearance of the nonlinear term in the energy expression, problems described by (14) and (17) are actually linear; (ii) we know in advance that $w^* = w^j$ and $\dot{u}^* = 0$, however, these quantities are still treated as unknowns in our scheme for the reason that w and u appeared here are local variables, defined within each element, which in general are different from the so-called global variables based on which actual calculations are conducted, refer to the Appendix B. As such, in most cases, we cannot directly assign values to w^* and $\dot{u}^*$; (iii) since the values of all variables are calculated/stored on discrete nodes, the same interpolation formula is used for representing w^* and w^j, as well as for u^* and u^j, based on their values at nodal points. As pointed out earlier, here a cubic interpolation of w within any element is used while a linear interpolation of u is adopted.

Buckling of a single bio-polymer filament

As an example, let's consider the compressive response a simply supported filament in the presence of thermal fluctuations. Specifically, we want to extract the relationship between the compressive strain and the force F needed to be applied on both ends as depicted in Fig. 2. Calculations were conducted by fixing one end of the filament and assigning an axial displacement of $-\Delta$ to the other end, i.e. $u(L) = -\Delta$. As such, a constant nominal compressive strain $\epsilon = \Delta/L$ was maintained in the simulation and the average axial force within filament was then calculated and monitored. Based on eight independent simulations, the average axial force, i.e. $< F >$, as a function of compressive strain is shown in Fig. 4 by the circular symbols. Notice that the force is normalized by the classic Euler buckling load $F_{c0} = \pi^2 EI/L^2$ and ϵ is normalized by the corresponding Euler buckling strain

$\epsilon_{c0} = \pi^2 EI/EAL^2$. Clearly, our results suggest that filament force reaches its maximum at certain moderate ϵ/ϵ_{c0} value, ~ 3 in Fig. 4, and then gradually drops to F_{c0} as the compressive strain continues to increase.

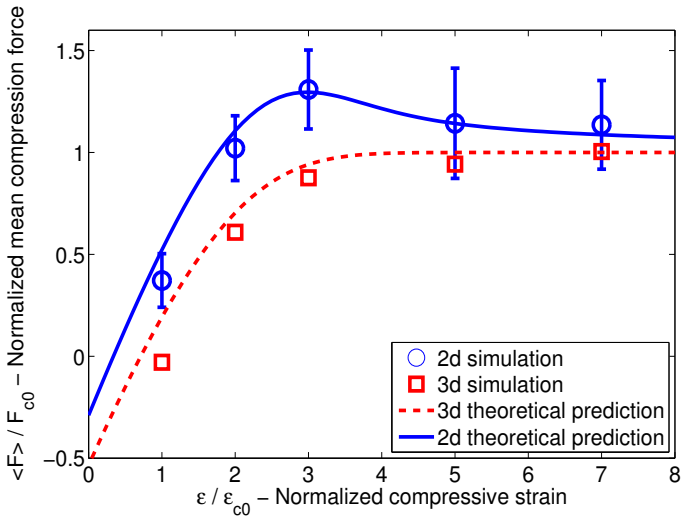

Figure 4: Filament force as a function of nominal compressive strain. Circular and square symbols correspond to results from eight independent 2d and 3d simulations, respectively. Theoretical predictions on this quantity are represented by the solid (for 2d) and dashed (for 3d) lines. Parameters chosen here are $\frac{EI}{k_B TL} = 100$ and $\frac{EAL}{k_B T} = 10^6$.

Actually, the same problem has been considered recently via modal analysis approach (Hu et al., 2012) and the prediction from that study is represented by the solid line in Fig. 4. Clearly, simulation results here match with the theoretical prediction very well. In particular, our results reproduce the right peak position as well as the correct peak value of the force. Of course, the formulation given by (13-18) is for the two-dimensional case only. However, it is straightforward to extend it to accommodate filament deformation in 3d. Specifically, we only need to introduce a new variable v, representing filament deflection in the third direction, and account for its contribution (similar to that of w) to the bending

and stretching energies, and finally add a random force in the third direction as well. The 3d simulation results are given in Fig. 4, demarcated by the square symbols. Unlike two dimensional cases, now the filament force asymptotically approaches F_{c0} but can never exceed it. Prediction from (Hu et al., 2012) on the filament force in 3d is also shown in Fig. 4 by the dashed line. Again, we can see that simulation results agree with theory rather well.

Mechanical response of actin networks

To further demonstrate the capability of the formulation and the corresponding numerical scheme proposed here, we then examine the mechanical behavior of a network consisting of randomly crosslinked actin filaments (each of length $\sim L$) as shown in Fig. 5. The lateral sides of the network are traction-free whereas the bottom is clamped to the ground, that is all degrees of freedom are fully constrained there. In addition, suppose that the top face of the network is attached to a rigid surface which moves in the horizontal direction with a distance Δ, refer to Fig. 5. Our goal is to find how the reaction force F that is applied on the rigid surface varies with the macroscopic strain defined as $\gamma = \Delta/(3L)$. We proceed by dividing the whole network into 141 elements and choosing $\frac{EI}{k_BTL} = 100$ and $\frac{EAL}{k_BT} = 10^6$, i.e. the same as those in Fig. 4. Recall that the persistence length of F-actin is believed to be of the order of 10-15μm (Boal, 2002) while its stretching rigidity, i.e. EA, has been reported to be around 35nN (Liu and Pollack, 2002), hence the combination $\frac{EI}{k_BTL} = 100$ and $\frac{EAL}{k_BT} = 10^6$ corresponds to an actin network with $L \approx 120$nm. At various fixed strain levels, that is keeping Δ constant, calculations are carried out by selecting a uniformly strained network as the starting configuration.

The average value of F from a typical simulation, at 0.02 percent macroscopic strain,

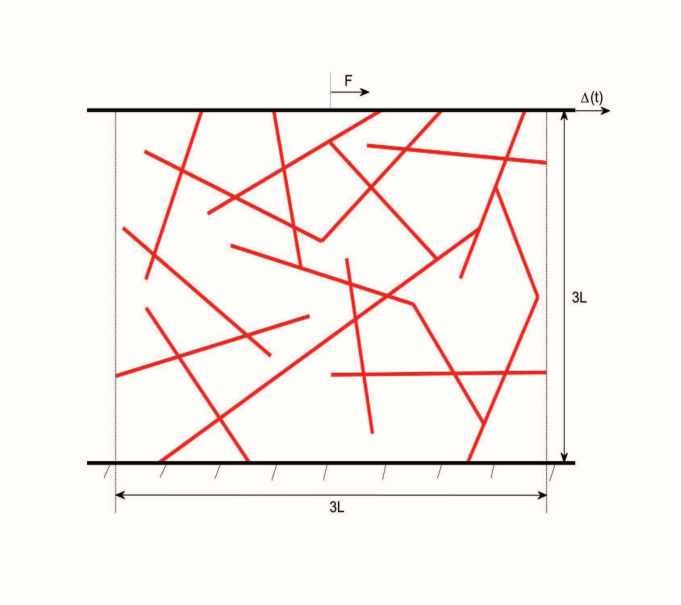

Figure 5: A random network consisting of multiple actin filaments undergoes simple shear deformation.

is shown in Fig. 6 by the solid line. In comparison, the values of this quantity obtained by neglecting thermal excitations (achieved by setting the random force f_i^j in (15) to zero) in the calculation are also given in Fig. 6. Clearly, $< F >$ quickly converges to a fixed value if entropy effect is neglected, refer to the inset of Fig. 6. In contrast, it takes much longer for this force, in the presence of thermal fluctuations, to reach a constant level and then oscillates around it. Interestingly, although the applied strain is positive, $< F >$ predicted here is actually negative. We must point out that this finding, i.e. the resistive force is negative at small strain, is by no means "universal". Instead, what this means physically is that, for this particular network, thermal excitations tend to tilt the structure to the right at zero applied force (because the architecture is not symmetric here and it is more difficult to shear the network to the left when compared to deform it to the right). The point we want to make is

that entropy will dictate how a filament network behaves when the deformation is small and hence, depending on the specific architecture, the average force exhibited by the network can be negative, refer to Fig. 6, as well as positive, as observed in several other networks we have examined (results not shown here). To verify that our FEM implementation agrees with predictions by standard finite-element software, we have compared our calculations with the results obtained from the FEM package Abaqus (adopting the same mesh size). Indeed, as shown in Fig. 6, our results are identical to the static prediction from Abaqus if entropy is neglected.

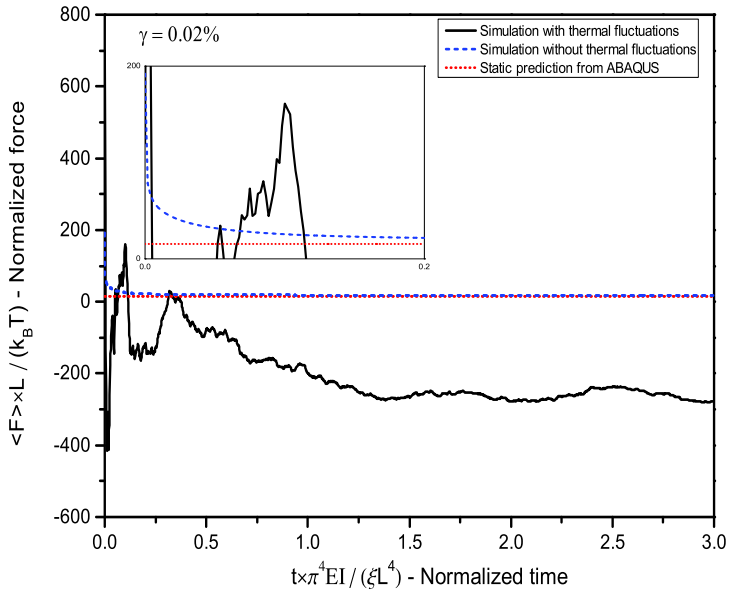

Figure 6: The average value of the net force acting on the network, under 0.02% macroscopic strain, as a function of simulation time.

To better illustrate the roles of entropy and enthalpy, i.e. elasticity, on how such actin networks behave, the macroscopic stress τ, defined as $\tau =< F > /(3L)^2$, as a function of strain is shown in Fig. 7a. Results presented here are based on four independent calculations

each with the same simulation time of $\pi^4 tEI/\xi L^4 = 8$. In addition, τ is normalized by G_0 which is the initial bulk shear modulus of the network. Notice that $\tau = \gamma G_0$ if thermal fluctuations are neglected and if there is no strain hardening.

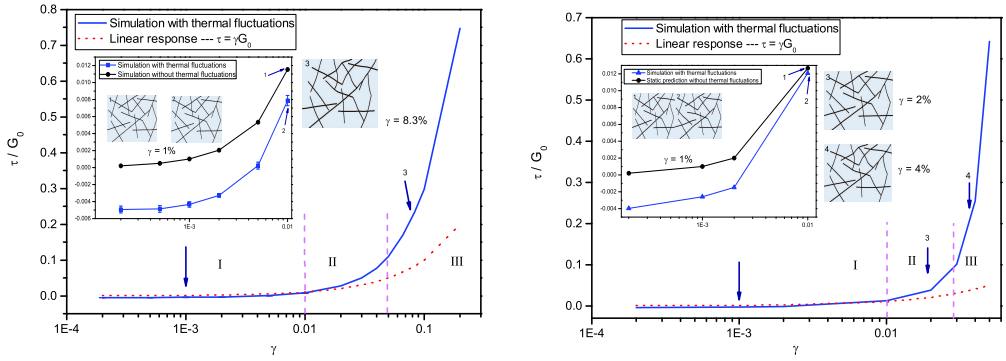

(a) (b)

Figure 7: The macroscopic shear stress within the network as a function of the applied strain. (a)-network with a mesh size of $L = 120$ nm; (b)-network with a mesh size of $L = 1.2$ μm. At small strain regime, the comparison between simulation results with and without considering thermal fluctuations is given in the inset. Snap shots showing the deformed shape the network, at various strain levels, are also provided. As strain increases, the network response changes from being entropy (regime I) to bending (regime II), and eventually, to stretching (regime III) dominated.

At this point, it is clear that τ significantly deviates from the value obtained by neglecting temperature effects when the applied strain is small, say less than 0.1%, refer to the inset of Fig. 7a. However, as γ increases, entropy effects become negligible and the mechanical response is governed by enthalpy. In addition, the network exhibits strain hardening as deformation increases. Specifically, we find that the hardening becomes significant when the stress level reaches $\sim 10\%$ of G_0. Close examination of the deformed structure, see the inset in Fig. 7a, suggests that the hardening is caused by the fact that small deformations can be accommodated by filament bending while direct stretching of some filaments

becomes inevitable at large strain, a well known phenomenon that has been reported in previous studies (Onck et al., 2005; Huisman et al., 2007). Hence, our results indicate that, as deformation progresses, the response of such actin network undergoes transitions from being entropy dominated to being governed by filament bending and, ultimately, to being dictated by filament stretching. Furthermore, the levels of macroscopic stress at which these transitions take place were found to be around 1 and 10 percent, respectively, of the initial bulk modulus of the network, refer to Fig. 7a.

We have also conducted simulations by increasing the network mesh size to $L = 1.2\mu m$, that is a 10-fold increase, and the results are shown in Fig. 7b. Basically, the same conclusion, i.e. the response changes from being fluctuations- to bending- and, eventually, to stretching-dominated, was obtained. Furthermore, the critical stress levels around which these transitions take place were, again, found to be $\sim 0.01G_0$ and $\sim 0.1G_0$ respectively. Since F-actin in biological cells have lengths ranging from 100nm-1μm in the so-called lamellipodium to a few micrometers in the main cell cortex (Fletcher and Mullins, 2010), results obtained here are expected to be relevant in interpreting measurement data on the mechanical properties of real cells. Indeed, Fernández and co-workers (Fernández et al., 2006) found that significant hardening takes place within 3T3 Fibroblasts when the stress level is above 10% of their initial moduli. The comparison between results obtained here and several sets of data reported in (Fernández et al., 2006) is shown in Fig. 8(a) and 8(b), where the deviation of network behavior from linear response is plotted against the applied stress. Notice that, in addition to the network shown in Fig. 5 (denoted as network 1 in Fig. 8), we have also conducted simulations on eight other random networks (with structures not shown here), seven of which containing the same number of filaments as that in Fig. 5 while the last one consisting of twice the number of F-actin filaments, and similar responses were

observed. We find that the computational results fit experimental data on the cytoskeleton in Fibroblasts very well (Fernández et al., 2006). The fact that results corresponding to different networks apparently collapse into a universal trend, refer to Fig. 8, suggests that conclusions obtained here should be rather general and robust.

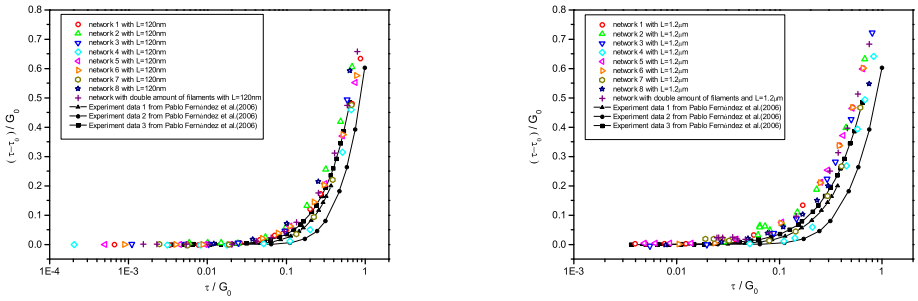

(a) (b)

Figure 8: Deviation of network behavior from linear response as a function of the applied stress level. Notice that G_0 is the initial bulk modulus of the network and $\tau_0 = \gamma G_0$, with γ being the applied strain. (a)-networks with the same mesh size of $L = 120$ nm; (b)-networks with the mesh size of $L = 1.2$ μm.

Besides stress, it is also informative to examine the degree of affinity of the network during deformation. Specifically, we can define the deviation from affine behavior as (Onck et al., 2005)

$$Afn = \frac{1}{N} \sum_{k=1}^{N} \frac{\|\Delta \mathbf{r}^k - \Delta \mathbf{r}^k_{aff}\|}{\|\Delta \mathbf{r}^k_{aff}\|}, \tag{19}$$

where N is the number of nodal points involved in the calculation, $\Delta \mathbf{r}^k$ is the displacement vector of nodal point k after the strain γ is applied while $\Delta \mathbf{r}^k_{aff} = [\gamma r^k_y \;\; 0]^T$ is the corresponding value if the deformation is affine with r^k_y being the y component of the position

vector of node k. For the network shown in Fig. 5, Afn as a function of the applied strain is given in Fig. 9 which demonstrates that the deformation is far away from being affine (i.e. $Afn >> 0$) at small strain but becomes increasingly affine-like as deformation progresses indicating that elasticity has taken over and become the dominant factor in this regime.

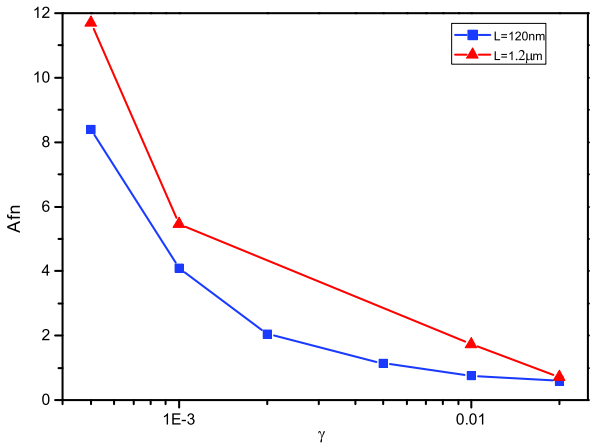

Figure 9: The deviation from affine behavior, Afn, as a function of the macroscopic strain.

One important feature of F-actin is that each monomer within the filament can bind to either ATP or ADP (after hydrolysis). Recent studies have suggested that F-ATP-actin and F-ADP-actin have different properties (Yogurtcu et al., 2012). In particular, it has been found that the persistence length of F-ADP-actin is around 9 μm (Isambert et al., 1995; McCullough et al., 2008; Greenberg et al., 2008), noticeably lower than that of F-ATP-actin ($\sim 12\mu$m). In addition, molecular dynamics simulations (Chu and Voth, 2006) indicated that the stretching rigidity of F-actin decreases by $\sim 16\%$ (from around 37 nN to 31 nN) after complete hydrolysis. Based on this information, we expect the normalized bending and stretching rigidities to become $\frac{EI}{k_BTL} \approx 75$ and $\frac{EAL}{k_BT} \approx 8.4 \times 10^5$ when all filaments in the network shown in Fig. 5 (with $L \approx 120$nm) change from F-ATP-actin to F-ADP-actin. The

influence of chemical state change of filament on the network response is given in Fig. 10 where we can clearly see that hydrolysis causes the network to become "softer" as expected.

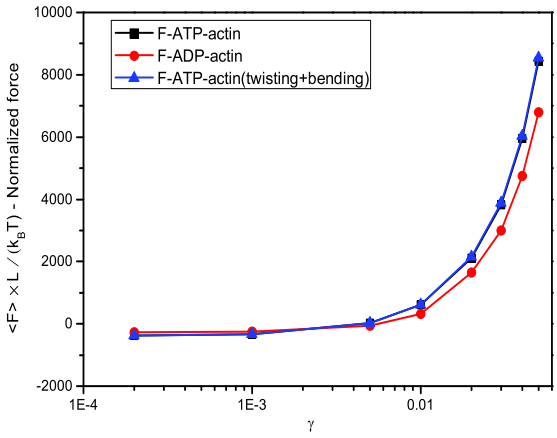

Figure 10: The influence of chemical state change, as well as twist, of filaments on the mechanical response of the network shown in Fig. 5 (with $L = 120nm$). The dimensionless parameters are chosen as $\frac{EI}{k_BTL} = 100$ and $\frac{EAL}{k_BT} = 10^6$ for F-ATP-actin; $\frac{EI}{k_BTL} = 75$ and $\frac{EAL}{k_BT} = 8.4 \times 10^5$ for F-ADP-actin; and $\frac{EI}{k_BTL} = 101$ and $\frac{EAL}{k_BT} = 10^6$ for F-ATP-actin (twisting+bending).

Another interesting factor to consider is the twist of filaments. Recently, De la Cruz et al. (2010) have proposed that the elastic energy density U_e stored in a F-actin subjected to both bending and twisting can be estimated as

$$\frac{2U_e}{k_BT} = L_B\kappa_1^2 + L_T\kappa_3^2 + 2L_{TB}\kappa_1\kappa_3 \tag{20}$$

where κ_1 and κ_3 are the curvature and twist (both having a unit of radian per unit length) in the 2D filament, respectively. L_B and L_T represent the so-called bending and torsional persistence lengths of F-actin. The last term on the right hand side of Eq. (20) describes the effect of twist-bend coupling in actin filaments. Furthermore, it has been estimated that the

values of L_T and L_{TB} for F-ATP-actin are around 1.4 and 0.4 μm respectively (De la Cruz et al., 2010). Eq. (20) suggests that when a torsionally unconstrained F-actin is undergoing bending deformation, spontaneous twist will be induced in the filament to minimize the strain energy. It can easily be shown that $2U_e/k_BT = (L_B - L_{TB}^2/L_T)\kappa_1^2$ when the minimum energy state is reached. In comparison, if the F-actin is fully constrained against twist (i.e. $\kappa_3 = 0$), then the strain energy density in the filament is simply $2U_e/k_BT = L_B\kappa_1^2$. At this point, it is clear that we just need to increase the effective bending rigidity EI from $(L_B - L_{TB}^2/L_T)k_BT$ to L_Bk_BT if all filaments in a 2D network change from being torsionally unconstrained to fully confined against twist (by, for example, rigid corsslinking proteins). However, such increase is very small (around 1%), given that $L_B/(L_B - L_{TB}^2/L_T) \approx 1.01$ for $L_B = 12\mu$m, and hence the influence of filament twist on the deformation of 2D networks should be negligible, as confirmed by the simulation results shown in Fig. 10. Of course, considering the effect of filament twist in a two-dimensional configuration will inevitably be ambiguous. To really answer this question, simulations on networks with realistic three-dimensional structures must be conducted.

It is noteworthy to mention that, besides finite element method (FEM), other computational approaches have also been developed to determine the deformation of semi-flexible networks. For example, Levine and co-workers (Head et al., 2003a; Bai et al., 2011) have discretized the network by assigning nodes at every crosslinking points, as well as the mid-points between each pair of adjacent crosslinks, and then estimated the strain energy in terms of the extension and angle rotation of each segment. Such approach is more efficient than FEM because, effectively, only the first bending mode between two neighboring crosslinks has been considered. However, in terms of accuracy, this method will not be as good as FEM especially for flexible networks where higher bending modes of individual

filament may contribute significantly to their bulk response. In addition, as pointed out earlier, modal analysis has been used by Van der Giessen and co-authors (Onck et al., 2005; Dillen et al., 2008) to introduce undulations of filaments in the network at its stress free state to represent the influence of entropy, a treatment greatly simplying/accelerating the calculation but, at the same time, overlooking the dynamic nature of thermal excitations.

We must point out that crosslinking points between filaments are treated as rigid and infinite strong in this study while, in reality, cross-linker proteins are deformable and their binding with F-actin can also be disrupted by force. In addition, the focus here is to examine how factors like entropy, filament bending, and filament stretching influence the behavior of networks while the role of other important players such as filament concentration and cross-linker density has not been investigated. Careful studies in the future are needed to address these important issues.

Concluding remarks

In this paper, we developed a numerical method to capture the thermal undulations of bio-polymers and then applied it to investigate the mechanical response of physiologically relevant actin networks. Main results of this study can be summarized as follows

- A Langevin dynamics based formulation is proposed to describe the shape fluctuations of bio-filaments. We show that, solutions of the resulting stochastic partial differential equation(SPDE) asymptotically reduce to predictions from classical modal analysis for simple problems and hence unambiguously provide support to this approach.
- Methods have been developed to implement the formulation in finite element (FEM) simulations where, in addition to entropy, the finite deflection of filament has also been

taken into account by introducing the well-known von Karman strain.

- The validity of the proposed finite element-Langevin dynamics (FEM-LD) approach is verified by comparing the simulation results on the behavior of a single filament with various theoretical predictions.

- As an application, our method is used to investigate the mechanical response of networks consisting of numerous randomly crosslinked F-actin. Simulation results indicated that, as deformation progresses, the response of such network undergoes transitions from being entropy dominated to being governed by filament bending and then, ultimately, to being dictated by filament stretching. Furthermore, the levels of macroscopic stress at which these transitions take place were found to be around 1 and 10 percent, respectively, of the initial bulk modulus of the network.

- Our results quantitatively agree well with experimental data on the strain-hardening behavior of Fibroblasts.

We expect that the FEM-LD approach proposed here to be very useful in simulating phenomena like actin-driven motility (Lin, 2009; 2010; Rafelski et al., 2009; Dayel et al., 2009; Lin et al., 2010) where thermal undulations of polymerizing filaments are thought to play a central role. In addition, it can also serve as a computational platform for future studies on the dynamics (Lieleg et al., 2010; 2011) or mechanical response (Hong et al., 2008; 2010) of biopolymer networks/gels where the influence of factors like the association/dissociation (Broedersz et al., 2010) and possible unfolding (Kim et al., 2009; 2011) of cross-linking proteins on the bulk viscoelastic rheological behavior of the network can be systematically examined. Investigations along these lines are in progress.

Acknowledgement

Y.L. is grateful for support from the Research Grants Council (Project No. HKU 7148/10E) of the Hong Kong Special Administration Region as well as a seed fund (Project No. 201011159154) from the University of Hong Kong. V.B.S. acknowledges support through a grant from the National Science Foundation (No. CMMI-1129172).

References

1. Arruda, E.M., and M.C. Boyce. 1993. A three-dimensional constitutive model for the large stretch behavior of rubber elastic materials. *J. Mech. Phys. Solids.* **41**: 389-412.

2. Bai, M., A.R. Missel, A.J. Levine, and W.S. Klug. 2011. On the role of the filament length distribution in the mechanics of semiflexible networks. *Acta Biomaterialia.* **47**: 2109-2118.

3. Boal, D. 2002. *Mechanics of the cell.* Cambridge University Press, Cambridge.

4. Broedersz, C.P., M. Depken, N.Y. Yao, M.R. Pollak, D.A. Weitz, and F.C. MacKintosh. 2010. Cross-link-governed dynamics of biopolymer networks. *Physical Review Letters.* **105**: 238101.

5. Broersma, S. 1960. Rotational diffusion constant of a cylindrical particle. *The Journal of Chemical Physics.* **32**: 1626-1631.

6. Chaudhuri, O., S.H. Parekh, and D.A. Fletcher. 2007. Reversible stress softening of actin networks. *Nature*. **445**: 295-298.

7. Chen, P., and V.B. Shenoy. 2010. Strain stiffening induced by molecular motors in active crosslinked biopolymer networks. *Soft Matter*. **6**: 3548-3561.

8. Chu, J.W., and G.A. Voth. 2006. Coarse-grained modeling of the actin filament derived from atomistic-scale simulations. *Biophys. J.* **90**: 1572-1582.

9. Coffey, W.T., Y.P. Kalmykov, and J.T. Waldron. 2004. The Langevin Equation: With Applications to Stochastic Problems in Physics, Chemistry and Electrical Engineering. 2^{nd} Ed. World Scientific, Singapore.

10. De la Cruz, E.M., J. Roland, B.R. McCullough, L. Blanchoin, and J.L. Martiel. 2010. Origin of twist-bend coupling in actin filaments. *Biophys. J.* **99**: 1852-1860.

11. Cyron, C.J., and W.A. Wall. 2009. Finite-element approach to Brownian dynamics of polymers. *Physical Review E*. **80**: 066704.

12. Cyron, C.J., and W.A. Wall. 2010. Consistent finite-element approach to Brownian polymer dynamics with anisotropic friction. *Physical Review E*. **82**: 066705.

13. Dayel, M.J., O. Akin, M. Landeryou, V. Risca, A. Mogilner, and R.D. Mullins. 2009. In Silico Reconstitution of Actin-Based Symmetry Breaking and Motility. *PLoS Biol.* **7**: e1000201.

14. van Dillen, T., P.R. Onck, and E. Van der Giessen. 2008. Models for stiffening in cross-linked biopolymer networks: A comparative study. *J. Mech. Phys. Solids*. **56**: 2240-2264.

15. Doi, M., and S.F. Edwards. 1994. The Theory of Polymer Dynamics. Clarendon press, Oxford.

16. Fernández, P., P.A. Pullarkat, and A. Ott. 2006. A Master Relation Defines the Nonlinear Viscoelasticity of Single Fibroblasts. *Biophys. J.* **90**: 3796-3805.

17. Fletcher, D.A., and R.D. Mullins. 2010. Cell mechanics and the cytoskeleton. *Nature.* **463**: 485-492.

18. Gardel, M.L., J.H. Shin, F.C. MacKintosh, L. Mahadevan, P. Matsudaira, and D.A. Weitz. 2004. Elastic behavior of cross-linked and bundled actin networks. *Science.* **304**: 1301-1305.

19. Greenberg, M.J., C.L. Wang, W. Lehman, and J.R. Moore. 2008. Modulation of actin mechanics by caldesmon and tropomyosin. *Cell Motil. Cytoskeleton.* **65**: 156-164

20. Head, D.A., A.J. Levine, and F.C. MacKintosh. 2003a. Deformation of cross-linked semiflexible polymer networks. *Physical Review Letters.* **91**: 108102.

21. Head, D.A., A.J. Levine, and F.C. MacKintosh. 2003b. Distinct regimes of elastic response and deformation modes of cross-linked cytoskeletal and semi-flexible polymer networks. *Physical Review E.* **68**: 061907.

22. Hong, W., X. Zhao, J. Zhou, and Z.G. Suo. 2008. A theory of coupled diffusion and large deformation in polymeric gels. *J. Mech. Phys. Solids.* **56**: 1779-1793.

23. Hong, W., X. Zhao, and Z.G. Suo. 2010. Large deformation and electrochemistry of polyelectrolyte gels. *J. Mech. Phys. Solids.* **58**: 558-577.

24. Hu, B., V.B. Shenoy, and Y. Lin. 2012. Buckling and enforced stretching of biofilaments. *J. Mech. Phys. Solids.* **60**: 1941-1951.

25. Huisman, E.M., T. van Dillen, P.R. Onck, and E. van der Gissen. 2007. Three-dimensional cross-linked F-actin networks: relation between network architecture and mechanical behavior. *Physical Review Letters.* **99**: 208103.

26. Isambert, H., P. Venier, A.C. Maggs, A. Fattoum, R. Kassab, D. Pantaloni, and M.F. Carlier. 1995. Flexibility of actin filaments derived from thermal fluctuations. Effect of bound nucleotide, phalloidin, and muscle regulatory proteins. *J. Biol. Chem.* **270**: 11437-11444.

27. Kim, T., W. Hwang, H. Lee, and R.D. Kamm. 2009. Computational Analysis of Viscoelastic Properties of Crosslinked Actin Networks. *PLoS Comput. Biol.* **5**: e1000439.

28. Kim, T., W. Hwang, and R.D. Kamm. 2011. Dynamic Role of Cross-linking Proteins in Actin Rheology. *Biophys. J.* **101**: 1597-1603.

29. Koenderink, G.H., Z. Dogic, F. Nakamura, P.M. Bendix, F.C. MacKintosh, J.H. Hartwig, T.P. Stossel, and D.A. Weitz. 2009. An active biopolymer network controlled by molecular motors. *Proceedings of the National Academy of Sciences.* **106**: 15192-15197.

30. Lieleg, O., M.M.A.E. Claessens, Y. Luan, and A.R. Bausch. 2008. Transient binding and dissipation in cross-linked actin networks. *Physical Review Letters.* **101**: 108101.

31. Lieleg, O., K.M. Schmoller, M.M.A.E. Claessens, and A.R. Bausch. 2009. Cytoskeletal polymer networks: viscoelastic properties are determined by the microscopic interaction potential of cross-links. *Biophysical Journal* **96**: 4725C4732.

32. Lieleg, O., M.M.A.E. Claessens, and A. R. Bausch. 2010. Structure and dynamics of cross-linked actin networks. *Soft Matter.* **6**: 218C225.

33. Lieleg, O., J. Kayser, G. Brambilla, L. Cipelletti, and A.R. Bausch. 2011. Slow dynamics and internal stress relaxation in bundled cytoskeletal networks. *Nature Mater.* **10**: 236C242.

34. Lin, Y. 2009. Mechanics model for actin-based motility. *Physical Review E.* **79**: 021916.

35. Lin, Y. 2010. A model of cell motility leading to biphasic dependence of transport speed on adhesive strength. *J. Mech. Phys. Solids.* **58**: 502-514.

36. Lin, Y., M. Inamdar, and L.B. Freund. 2008. The competition between Brownian motion and adhesion in soft materials. *J. Mech. Phys. Solids.* **56**: 241-250.

37. Lin, Y., V.B. Shenoy, B. Hu, and L. Bai. 2010. A Microscopic Formulation for the Actin-Driven Motion of Listeria in Curved Paths. *Biophys. J.* **99**: 1043-1052.

38. Liu, A., D.L. Richmond, L. Maibaum, S. Pronk, P.L. Geissler, and D.A. Fletcher. 2008. Membrane-induced bundling of actin filaments. *Nature Physics.* **4**: 789-793.

39. Liu, X., and G.H. Pollack. 2002. Mechanics of F-actin characterized with microfabricated cantilevers. *Biophys. J.* **83**: 2705-2715.

40. MacKintosh, F.C., J. Kas, and P.A. Janmey. 1995. Elasticity of semiflexible biopolymer networks. *Physical Review Letters.* **75**: 4425-4428.

41. Mark, J.E., and E.B. Erman. 1988. Rubberlike Elasticity: a Molecular Primer. Wiley, New York.

42. Marko, J.F., and E.D. Siggia. 1995. Stretching DNA. *Marcomolecules.* **28**: 8759-8770.

43. Mattila, P.K., and T. Lappalainen. 2008. Actin Filopodia: molecular architecture and cellular functions. *Nature Reviews Molecular Cell Biology.* **9**: 446-454.

44. McCullough, B.R., L. Blanchoin, J.L. Martiel, and E.M. De la Cruz. 2008. Cofilin increases the bending flexibility of actin filaments: implications for severing and cell mechanics. *J. Mol. Biol.* **381**: 550-558.

45. Milner, S.T., and S.A. Safran. 1987. Dynamical fluctuations of droplet microemulsions and vesicles. *Physical Review A.* **36**: 4371-4379.

46. Ockendon, H., and J.R. Ockendon. 1995. Viscous Flow. Cambridge University Press, New York.

47. Onck, P.R., T. Koeman, T. van Dillen, and E. Van der Giessen. 2005. Alternative explanation of stiffening in cross-linked semiflexible networks. *Physical Review Letters.* **95**: 178102.

48. Palmer, J.S., and M.C. Boyce. 2008. Constitutive modeling of the stress-strain behavior of F-actin filament networks. *Acta Biomaterialia.* **4**: 597-612.

49. Preston, T.M., C.A. King, and J.S. Hyams. 1990. The Cytoskeleton and Cell Motility. Blackie, Glasgow.

50. Rafelski, S.M., J.B. Alberts, and G.M. Odell. 2009. An Experimental and Computational Study of the Effect of ActA Polarity on the Speed of Listeria monocytogenes Actin-based Motility. *PLoS Comput. Biol.* **5**: e1000434.

51. Reddy, J.N. 1993. An Introduction to the Finite Element Method. 2nd ed. McGraw-Hill, New York.

52. Reddy, J.N. 2004. An Introduction to Nonlinear Finite Element Analysis. Oxford University Press, New York.

53. Storm, C., J.J. Pastore, F.C. MacKintosh, T.C. Lubensky, and P.A. Janmey. 2005. Nonlinear elasticity in biological gels. *Nature*. **435**: 191-194.

54. Tharmann, R., M.M.A.E. Claessens, and A.R. Bausch. 2007. Visceoelasticity of isotropically cross-linked actin networks. *Physical Review Letters*. **98**: 088103.

55. Theriot, J.A., and T.J. Mitchison. 1991. Actin microfilament dynamics in locomoting cells. *Nature*. **352**: 126-131.

56. Tritton, D.J. 1988. Physical Fluid Dynamics. Oxford University Press, New York.

57. Wagner, B., R. Tharmann, I. Haase, M. Fischer, and A.R. Bausch. 2006. Cytoskeletal polymer networks: the molecular structure of cross-liners determines macroscopic properties. *Proceedings of the National Academy of Sciences*. **103**: 13974-13978.

58. Wilhelm, J., and E. Frey. 2003. Elasticity of stiff polymer networks. *Physical Review Letters*. **91**: 108103.

59. Yogurtcu, O.N, J.S. Kim, and S.X. Sun. 2012. A Mechanochemical Model of Actin Filaments. *Biophys. J.* **103**: 719-727.

Appendices

Appendix-A

To determine the viscous coefficient ξ and ξ_{ax} introduced in our formulation, we have to estimate the drag force acting on an infinite cylinder moving transversely as well as longitudinally in the fluid, as shown in Fig. A1. The governing equations in this case are (Ockendon and Ockendon, 1995)

$$\rho\left[\frac{\partial \mathbf{u}}{\partial t} + (\mathbf{u}\cdot\nabla)\mathbf{u}\right] = -\nabla p + \mu\nabla^2\mathbf{u}, \tag{A1}$$

and

$$\nabla\cdot\mathbf{u} = 0 \tag{A2}$$

where $\mathbf{u}$ is the velocity vector, t represents time, p is the pressure, ρ and μ are the density and viscosity of the the fluid, respectively. Notice that (A1) is the famous Navier-Stokes equation and (A2) comes from the assumption that the fluid is incompressible.

The problem depicted in Fig. A1(a) has been considered by various researchers. Specifically, when the so-called Reynolds number (i.e. $2\rho Va/\mu$) is small, the steady state drag force (per unit length) acting on the cylinder has been found to be of the order of $4\pi\mu V$ (Tritton, 1988; Ockendon and Ockendon, 1995). Hence, we can estimate that the value of ξ is around $4\pi\mu$. For the case where the cylinder is moving along the longitudinal direction as shown in Fig. A1(b), the problem is axisymmetric and so, at steady state, the velocity and pressure fields can be expressed as (in the cylindrical coordinates)

$$\mathbf{u} = u_z(r)\vec{\mathbf{e}}_z, \qquad p = p(r) \tag{A3}$$

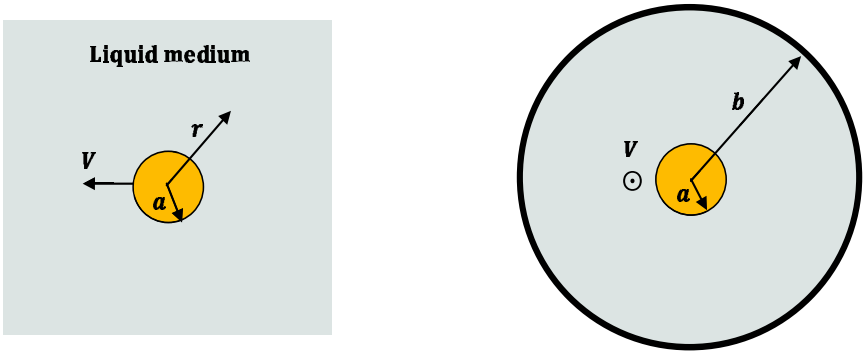

Figure A1: Schematic plot of an infinite-long cylinder (with radius a) moving transversely (a), as well as longitudinally (b), with a velocity V in the fluid.

where $\vec{\mathbf{e}}_z$ is the unit vector along the axial direction. Notice that since we are dealing with an infinite cylinder, $\mathbf{u}$ and p are not expected to depend on z. To estimate the frictional force, assume that there is a stationary boundary at $r = b$ where the fluid velocity drops to zero. In this case, the solutions are

$$u_z(r) = \frac{\ln(b/r)}{\ln(b/a)} V, \qquad p = p_0. \tag{A4}$$

The drag force acting on the cylinder can then be calculated as

$$f_z = 2\pi a\mu \frac{du_z(r)}{dr} \mid_{r=a} = -\frac{2\pi\mu}{\ln(b/a)} V \tag{A5}$$

where the negative sign stands for the fact that the frictional force is opposite to the direction of motion. In light of (A5), ξ_{ax} can be found as $\xi_{ax} = \frac{2\pi\mu}{\ln(b/a)}$. Recall that the conclusion that $\xi \sim 4\pi\mu$ is obtained by considering a long cylinder moving transversely in an *infinite*

fluid medium (Tritton, 1988; Ockendon and Ockendon, 1995). Hence, to be self-consistent, we must take b/a to be very large when comparing the values of ξ_{ax} and ξ. At this point, it is clear that the viscous coefficient associated with the axial movement of a filament segment should be much smaller than that corresponding to its transverse motion, that is $\xi_{ax} << \xi$. A simple explanation is given in Fig. A2 where the relative motion of medium molecules with respect to the cylinder is illustrated. Basically, liquid molecules near a cylinder moving transversely must change their moving speed and direction, as shown in Fig. A2(a), leading to a relatively high macroscopic drag force. In contrast, at steady state, medium molecules near a cylinder surface will not be significantly disturbed by its axial movement (instead, they just move along with the cylinder), refer to Fig. A2(b). As a result, the frictional force acting on the cylinder is expected to be very small in this case.

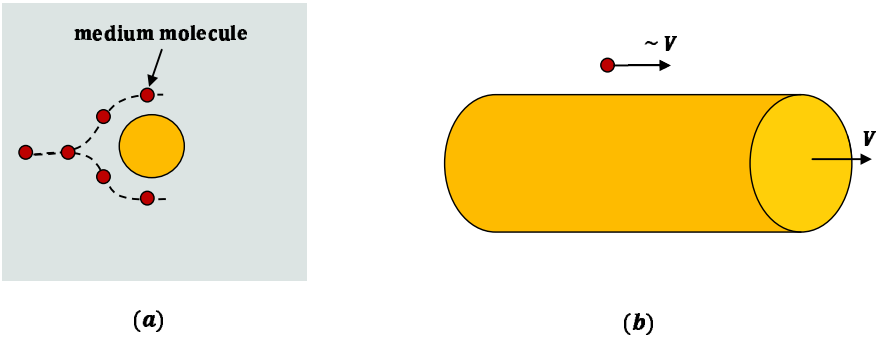

Figure A2: Illustration of the relative motion of medium molecules with respect to the moving cylinder. (a)-liquid molecules (small circles) must change their speed and moving direction to circulate around an infinite cylinder moving transversely. (b)-for an infinite cylinder moving along the longitudinal direction, liquid molecules near its surface do not need to change their motions, instead they just keep moving along with the cylinder.

It must be pointed out that the conclusion obtained here (i.e. the drag coefficient of a filament segment moving along the axial direction of the rod is much smaller than that of the

same segment moving perpendicular to the filament) is different from that by considering the *free diffusion* of a rod, as depicted in Fig. A3(a), where the drag forces prevent the whole rod from moving longitudinally and transversely, respectively, have been found to be within a factor of two of each other (Broersma, 1960; Cyron and Wall, 2009; 2010). However, we believe that our approach is more appropriate for examining the *mechanical response* of biopolymer networks for several reasons

- First of all, unconstrained rigid body motions (i.e. linear translation and rotation) of the filament are inadmissible in analyzing the deformation of biopolymer networks (or any other solid structures for that matter) because of the confinement at the boundaries and the fact that different filaments are connected to each other. Therefore motion of a segment is determined by the displacement of its neighbors; as such, the scenarios shown in Fig. A3(a) are not directly relevant here. To make this point clear, let's consider the network shown in Fig. A3(b) where three filaments crosslink to form an equilateral triangle with all corners fully constrained against displacement. Evidently, no linear translation or rotation of the whole filament is possible/allowed when examining the deformation of such structure. Instead, we should look at the movement of a segment *within* a filament (that is, not an *isolated* cylinder with two end faces exposed to the medium) which, we believe, is consistent with the two-dimensional treatment of the problem adopted here.

- More importantly, a natural consequence of using the picture shown in Fig. A3(a) to estimate the viscous force acting on the filament is that the drag coefficients obtained there inevitably depend on the total length, L, of the rod (Broersma, 1960; Cyron and Wall, 2009; 2010) which will introduce serious consistency problems when applied to

study the mechanical behavior of networks. For example, following this logic, drag forces acting on three segments, each with the same element size Δx and located at the centers of each side of the equilateral triangle shown in Fig. A3(b), will be different even if they all move with the same transverse speed (just because the three filaments have different lengths, i.e. $L_1 \neq L_2 \neq L_3$). However, in light of the symmetry (recall that all corners of the equilateral triangle are constrained against displacement), the magnitudes of these frictional forces are expected to be the same from a physical point of view. This problem will become serious when, for example, in vivo actin networks are considered where the length of F-actin can range from several tens of nanometers to several microns. In comparison, such an issue will not appear if our approach is adopted (that is, both ξ and ξ_{ax} are independent of the total filament length from our formulation, refer to Eq. (A5) and subsequent discussions).

- Finally, although we feel that it is more appropriate to take ξ_{ax} as much smaller than ξ, we have, nevertheless, conducted additional simulations by assigning non-vanishing values of ξ_{ax}. Notice that in this case a random axial force f_{ax}, which relates to ξ_{ax} via a relationship similar to that given in Eq. (1), acting on the filament also needs to be introduced in the calculation. Specifically, we examined the mechanical response of a single filament, as shown in Fig. 2, when ξ_{ax}/ξ equals to 0.2, 0.5, and 1 respectively. Choosing the same parameters as those in Fig. 4, the mean square of filament deflection at the mid-point (that is $< w(L/2)^2 >$) under zero nominal strain, i.e. $\epsilon = 0$, against time is shown in Fig. A4. Interestingly, simulation results corresponding to different ξ_{ax}/ξ values all converge to the same level. Based on eight independent calculations, the average of $< w(L/2)^2 >$, as well as its deviation, as a

function of ξ_{ax}/ξ is plotted in Fig. A5(a). Similarly, the dependence of the axial force F within filament, refer to Fig. 2, on ξ_{ax} is illustrated in Fig. A5(b). Clearly, our results suggest that the exact value of the longitudinal drag coefficient does not affect the long-term response of the system.

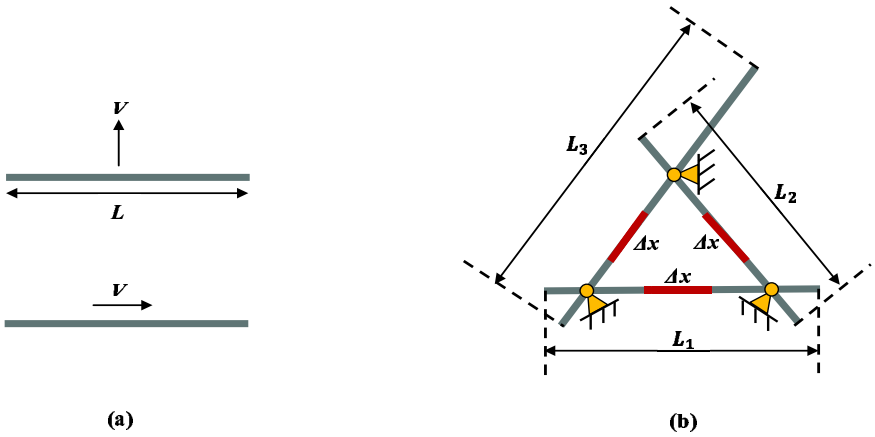

Figure A3: (a)-Standard picture for estimating drag forces on a rod under free diffusion. (b)-A network consisting of three corsslinked filaments with different lengths. An equilateral triangle is formed within the network with three corners constrained against displacement. Three elements, at the centers of each side of the triangle and with the same size Δx, are highlighted in red.

Appendix-B

In our FEM formulation, a cubic interpolation of w and a linear interpolation of u are adopted. In other words, it is assumed that, within element i, the displacement fields can be expressed as

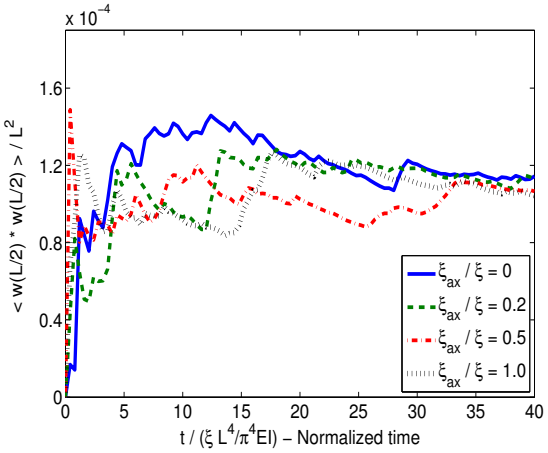

Figure A4: Mean square of filament deflection at mid-point under zero nominal strain (i.e. $\epsilon = 0$, refer to Fig. 2). The parameters chosen here are the same as those in Fig. 4.

$$w(x) = \phi_1(x)w_i + \phi_2(x)\theta_i + \phi_3(x)w_{i+1} + \phi_4(x)\theta_{i+1}, \quad u(x) = \psi_1(x)u_i + \psi_2(x)u_{i+1} \tag{B1}$$

with $\theta = -dw/dx$ and

$$\begin{aligned}
&\phi_1(x) = 1 - 3\left(\frac{x-x_i}{\Delta x}\right)^2 + 2\left(\frac{x-x_i}{\Delta x}\right)^3, \quad \phi_2(x) = -(x-x_i)\left(1 - \frac{x-x_i}{\Delta x}\right)^2 \\
&\phi_3(x) = 3\left(\frac{x-x_i}{\Delta x}\right)^2 - 2\left(\frac{x-x_i}{\Delta x}\right)^3, \quad \phi_4(x) = -(x-x_i)\left[\left(\frac{x-x_i}{\Delta x}\right)^2 - \frac{x-x_i}{\Delta x}\right] \\
&\psi_1(x) = 1 - \frac{x-x_i}{\Delta x}, \qquad\qquad \psi_2(x) = \frac{x-x_i}{\Delta x}
\end{aligned} \tag{B2}$$

where $\Delta x = x_{i+1} - x_i$ with x_i and x_{i+1} being the coordinates of the two ends of the element. Let $\mathbf{N}(x) = [\psi_1(x)\ \ \phi_1(x)\ \ \phi_2(x)\ \ \psi_2(x)\ \ \phi_3(x)\ \ \phi_4(x)]^T$, then the non-vanishing components

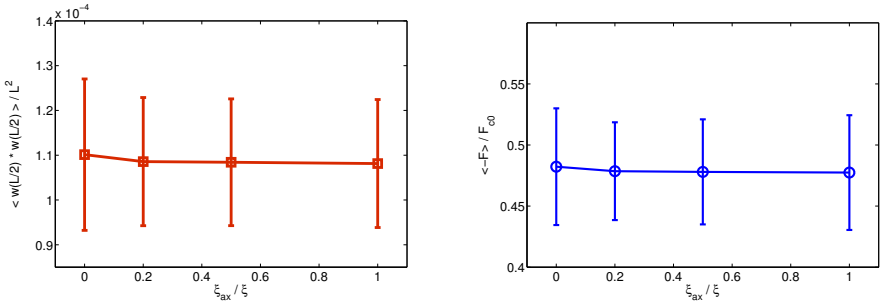

(a) (b)

Figure A5: (a)-$< w(L/2)^2 >$ as a function of ξ_{ax}/ξ. (b)-The dependence of average filament force on ξ_{ax}/ξ (notice that $< F >$ is negative here indicating that this force is tensile). Results shown here are based on eight independent simulations with the nominal strain of filament being zero.

of various matrices/vectors defined in (14) can be found as

$$K_{pq} = EA\int_{x_i}^{x_{i+1}} \frac{dN_p}{dx}\frac{dN_q}{dx}dx, \quad K_{mm} = \lambda, \quad A_{mm} = -\lambda$$
$$B_{pmn} = \frac{EA}{2}\int_{x_i}^{x_{i+1}} \frac{dN_p}{dx}\frac{dN_m}{dx}\frac{dN_n}{dx}dx, \quad F_p^u = \int_{x_i}^{x_{i+1}} f_u^{ext} N_p(x)dx \tag{B3}$$

where p(or q)$= 1, 4$ and m(or n)$= 2, 3, 5, 6$. λ is a large number (much bigger than other components in $\mathbf{K}$) introduced to enforce $w^* = w^j$ as specified in (13). Similarly, the non-vanishing components of various matrices/vectors introduced in (17) are

$$M_{mn} = \xi\int_{x_i}^{x_{i+1}} N_m(x)N_n(x)dx, \quad M_{pp} = \lambda, \quad C_{mn} = EI\int_{x_i}^{x_{i+1}} \frac{d^2N_m}{dx^2}\frac{d^2N_n}{dx^2}dx$$
$$D_{mpn} = EA\int_{x_i}^{x_{i+1}} \frac{dN_m}{dx}\frac{dN_p}{dx}\frac{dN_n}{dx}dx, \quad E_{mnrs} = \frac{EA}{2}\int_{x_i}^{x_{i+1}} \frac{dN_m}{dx}\frac{dN_n}{dx}\frac{dN_r}{dx}\frac{dN_s}{dx}dx$$

$$F_m^w = \int_{x_i}^{x_{i+1}} \left(f_i^j + f_w^{ext} \right) N_m(x) dx \tag{B4}$$

where, again, $p = 1, 4$ and m(or n, r, s)$= 2, 3, 5, 6$. f_w^{ext} represents the externally applied transverse load on element i. Since increments in u and w are calculated separately in our scheme, special attention must be paid to junction points where multiple filaments crosslink with each other as illustrated in Fig. B1. Let's focus our attention on element i (shown in Fig. B1) which shares a common node with elements from another filament. The first thing we need to consider is that, in this case, the axial displacement u_i of the common node, defined in element i, also partially represents the deflection, i.e. w, defined in other elements (such as element r in Fig. B1), suggesting that $\dot{u}_i^*$ should not be zero when calculating the velocity field in the second step of our scheme. As such, modifications to $\mathbf{M}$, given in (B4), must be made as

$$M_{11} = \lambda J(i, 1), \quad \text{and} \quad M_{44} = \lambda J(i, 2) \tag{B5}$$

where $J(i, 1) = 0$ if the first node in element i is a junction point while equals to 1 otherwise. Similarly, $J(i, 2)$ will be non-vanishing (equals to 1) only when node 2 of the element is not a crosslinking point. In addition to displacement, we also need to consider forces generated at junction points. As depicted in Fig. B1, the axial force f_{ax}^i generated within element i will contribute to the bending of the other filament and hence must be taken into account in the force vector $\mathbf{F}^w$, defined in (B4), as

$$F_1^w = EA\left[\frac{u_{i+1}^* - u_i^*}{x_{i+1} - x_i} + \frac{(\theta_i^*)^2}{2}\right][1-J(i,1)], \quad \text{and} \quad F_4^w = -EA\left[\frac{u_{i+1}^* - u_i^*}{x_{i+1} - x_i} + \frac{(\theta_{i+1}^*)^2}{2}\right][1-J(i,2)]. \tag{B6}$$

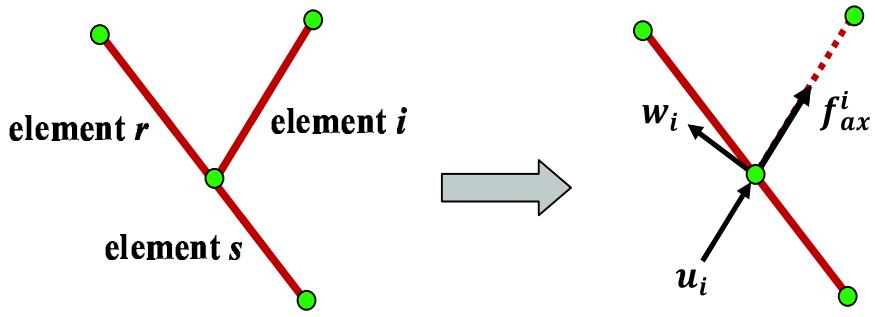

Figure B1: Schematic plot of a junction point within the network.

Another issue we must point out is that the vector χ appeared in (14) and (17) contains variables defined in the local coordinate system (attached to the element itself) which in general can be different from the so-called global variables, defined in a fixed reference frame (refer to Fig. B2), based on which actual calculations are conducted. Introducing a new vector $\hat{\chi} = \begin{bmatrix}\hat{u}_i & \hat{w}_i & \hat{\theta}_i & \hat{u}_{i+1} & \hat{w}_{i+1} & \hat{\theta}_{i+1}\end{bmatrix}^T$ with the hat symbol indicating that the variable is defined in the global reference frame, the transformation between χ and $\hat{\chi}$ can be achieved by

$$\chi = \mathbf{T} \cdot \hat{\chi} \tag{B7}$$

where $\mathbf{T}$ is a 6×6 transformation matrix defined as (Reddy, 1993)

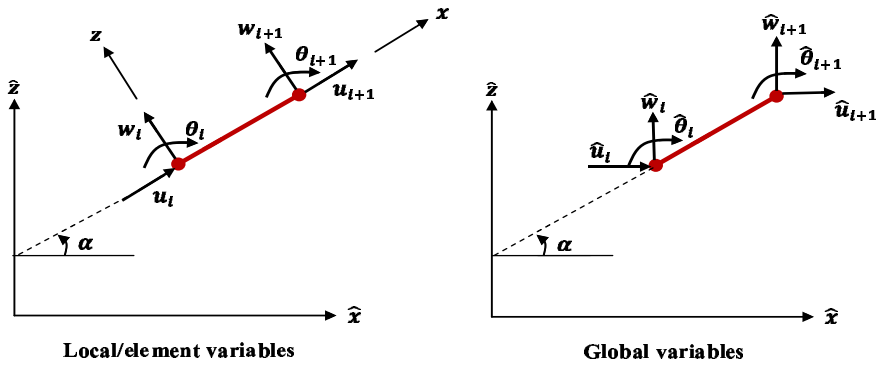

Figure B2: Definition of local and global degrees of freedom as well as their relationship.

$$T_{11} = T_{22} = T_{44} = T_{55} = \cos\alpha, \quad T_{33} = T_{66} = 1$$
$$T_{12} = -T_{21} = T_{45} = -T_{54} = \sin\alpha \tag{B8}$$

with α being the rotation angle between the local and global frames, refer to Fig. B2. As such, in terms of global variables, (14) can be rewritten as

$$\sum_i \delta\hat{\chi}_m^* \left[\hat{K}_{mn}\hat{\chi}_n^* + \hat{A}_{mn}\hat{\chi}_n^j + \hat{B}_{mnr}\hat{\chi}_n^j\hat{\chi}_r^j - \hat{F}_m^u\right] = 0 \tag{B9}$$

where

$$\hat{K}_{ij} = T_{ki}K_{kl}T_{lj}, \quad \hat{A}_{ij} = T_{ki}A_{kl}T_{lj}$$
$$\hat{B}_{ijk} = T_{li}B_{lmn}T_{mj}T_{nk}, \quad \hat{F}_i^u = T_{ji}F_j^u. \tag{B10}$$

Similarly, (17) can be transformed to

$$\sum_i \delta\hat{\chi}_m^* \left[\hat{M}_{mn}\dot{\hat{\chi}}_n^* + \hat{C}_{mn}\hat{\chi}_n^* + \hat{D}_{mnr}\hat{\chi}_n^*\hat{\chi}_r^* + \hat{E}_{mnrs}\hat{\chi}_n^*\hat{\chi}_r^*\hat{\chi}_s^* - \hat{F}_m^w\right] = 0 \tag{B11}$$

with

$$\begin{aligned} &\hat{M}_{ij} = T_{ki}M_{kl}T_{lj}, \quad \hat{C}_{ij} = T_{ki}C_{kl}T_{lj}, \quad \hat{F}_i^w = T_{ji}F_j^w \\ &\hat{D}_{ijk} = T_{li}D_{lmn}T_{mj}T_{nk}, \quad \hat{E}_{ijkl} = T_{mi}E_{mnpq}T_{nj}T_{pk}T_{ql}. \end{aligned} \tag{B12}$$

Notice that all subscript indices in (B10) and (B12) can assume values from 1 to 6. Finally, in order to reduce memory cost, only the non-vanishing components of these matrices are stored during the calculation.